Analytica Chimica Acta xxx (xxxx) xxx

Contents lists available at ScienceDirect

Analytica Chimica Acta

journal homepage: www.elsevier.com/locate/aca

Peptide-induced aggregation of glutathione-capped gold nanoclusters: A new strategy for designing aggregation-induced enhanced emission probes

Jyun-Guo You [a], Wei-Lung Tseng [a, b, c, *]

[a] Department of Chemistry, National Sun Yat-sen University, Taiwan, ROC
[b] School of Pharmacy, College of Pharmacy, Kaohsiung Medical University, Taiwan, ROC
[c] Center for Nanoscience and Nanotechnology, National Sun Yat-sen University, Taiwan, ROC

HIGHLIGHTS

- The AG73 peptide-GSH-AuNCs aggregates are suitable for sensing plasma heparin.
- The glycine-arginine repeat peptide-GSH-AuNCs aggregates are used to detect urinary trypsin.
- Alkaline phosphatase-induced hydrolysis of phosphopeptide that drives the AIEE of the GSH-AuNCs.
- The RGDR5-GSH-AuNC aggregates can recognize αvβ3 integrin-positive cells.

GRAPHICAL ABSTRACT

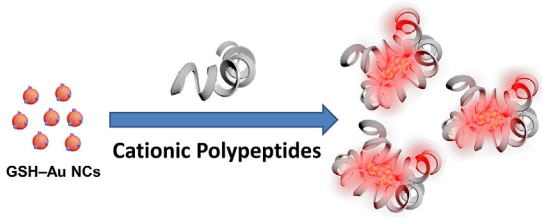

ARTICLE INFO

Article history:
Received 7 May 2019
Received in revised form
23 May 2019
Accepted 28 May 2019
Available online xxx

Keywords:
Glutathione-capped gold nanoclusters
Aggregation-induced enhanced emission
Peptides
αvβ3 integrin

ABSTRACT

A series of polymers and metal ions have been observed to be useful in triggering aggregation-induced emission (AIE) and AIE enhancement (AIEE) of thiolated gold nanoclusters (AuNCs). However, peptide-induced AIEE of thiolated AuNCs and their applications in biosensors have rarely been investigated. In this study, we showed that positively charged peptides induced efficient AIEE of negatively charged glutathione-capped AuNCs (GSH-AuNCs) through electrostatic attraction. In contrast to GSH-AuNCs, polyarginine (polyArg), a cationic peptide, stimulated the AIEE of the GSH-AuNCs, resulting in a 3.5-fold luminescence enhancement, 10-fold enhancement in quantum yield, 8-nm blueshift in the luminescence maximum, and a 2.1-fold increase in the mean luminescence lifetime. Four different AIEE-based biosensors with excellent selectivity and acceptable sensitivity were fabricated using cationic peptides as an AIEE-active trigger and as a biorecognition element. A heparin biosensor with a limit of detection (LOD) of 3 nM was constructed by combining AG73 peptide-mediated AIEE of the GSH-AuNCs and the specific interaction of AG73 peptides with heparin macromolecules. The concentration of human trypsin was selectively detected at a concentration as low as 1 nM using an arginine-glycine repeat peptide as an enzymatic substrate and as an AIEE-active trigger. Alkaline phosphatase (ALP)-catalyzed dephosphorylation of phosphopeptides paired with the corresponding product-mediated AIEE of the GSH-AuNCs was used for ALP sensing with an LOD of 0.3 U L^{-1}. A peptide consisting of a cyclic RGD unit and an AIEE-active unit was designed to synthesize RGD-modified GSH-AuNC aggregates that can target αvβ3 integrin receptors. These AIEE-based sensors were practically applied for the quantitative

* Corresponding author. Department of Chemistry, National Sun Yat-sen University, 70, Lien-hai Road, Kaohsiung, 804, Taiwan, ROC.
E-mail address: tsengwl@mail.nsysu.edu.tw (W.-L. Tseng).

https://doi.org/10.1016/j.aca.2019.05.069

determination of heparin in human plasma, trypsin in human urine, and ALP in human plasma as well as for luminescent imaging of αvβ3 integrin-overexpressing HeLa cells.

1. Introduction

Thiolate-protected gold nanoclusters (AuNCs) have received considerable interest for their potential applications in catalysis [1], sensing [2], optical and electronic devices [3], bioimaging [2], drug delivery [4], and artificial enzyme mimics [5,6]. They have been shown to possess molecule-like properties, such as molecular chirality [7], intrinsic magnetism [8], quantized charging [9], and photoluminescence (PL) [10]. Among the assorted molecular-like properties of thiolated AuNCs, PL is one of the most exciting features compared to previously reported nanomaterials. Similar to widely used semiconductor quantum dots, AuNCs offer size-, ligand- and structure-dependent PL properties with tunable emission (from the ultraviolet to near-infrared region) and a large Stokes shift [10]. In addition, recent studies have shown the unique PL properties of AuNCs, including long-lifetime luminescence (>100 ns) [11] and large two-photon absorption cross-sections [12]. These PL features combined with the low toxicity of gold enable AuNCs to detect an analyte of interest and local environmental variations (e.g., pH, temperature, and viscosity) in live cells and animals [13]. Moreover, AuNCs serve as a luminescence turn-on and turn-off probe for sensitive and selective detection of heavy metal ions [14], inorganic anions [15], small biomolecules [16], proteins [17], DNA [18], and enzyme-substrate catalytic reactions [19]. Nevertheless, most thiolate-protected AuNCs have a relatively low quantum yield (QY) of <1% and a low molar extinction coefficient, resulting in poor brightness. This weakness causes AuNCs to suffer from a low signal-to-background ratio in live cell imaging and biosensing platforms. Accordingly, strategies for enhancing the QY of thiolate-protected AuNCs are urgently needed, especially for the detection and imaging of low concentrations of a target analyte. To address this need, several researchers have used a variety of approaches to improve the QY of thiolate-protected AuNCs. These approaches are mainly classified into the following three categories: (1) tailoring of AuNCs with suitable capping ligands to tune the ligand-to-metal charge transfer process [20], (2) doping of AuNCs with metal ions to adjust the metal composition [21], and (3) aggregation-induced emission (AIE) and AIE enhancement (AIEE) of thiolate-stabilized AuNCs [22]. Since AIE- and AIEE-type AuNCs offer the distinct advantages of easy handling, a tunable QY, a switchable PL, and a controllable particle size, they are frequently used in the fields of optical sensors [23], light-emitting diodes [24], biomedical imaging [25], and drug delivery [25]. Polymer and metal ion-induced AIE and AIEE of AuNCs have been exemplified by poly(allylamine hydrochloride) [25], chitosan [26], polyetherimide [27], Gd(III) [22], Cd(II) [28], Pb(II) [5,23], Ag(I) [29], Ce(III) [30], and Zn(II) [31]. In the procedure concerning AIE and AIEE, AuNCs are initially synthesized *via* the reduction of the gold ion precursor using capping ligands. AuNCs are composed of a metal core protected by a layer of an Au(I)-thiolate complex [28]. The next step involves solvent-metal ion-, pH- and polymer-triggered assembly of the AuNCs [32], enhancing their PL. In contrast to AuNCs, assembled AuNCs exhibit a relatively high QY, long PL lifetime, and short emission wavelength [30].

Peptides, which are natural or synthetic short polymers of amino acids, have specific sequences, high stability, and broad chemical versatility and can be easily modified, enabling them to bind to particular analytes with high affinity and excellent selectivity [33]. This unique property allows peptides to behave as recognition elements in biosensors. In response to a binding event, a biosensor requires conjugation of a signal reporter, such as fluorophores [34], metal nanoparticles [35], quantum dots [36], carbon-based materials [37] polydiacetylene liposomes [38], lanthanide chelators [39], ferrocene [40], and methylene blue [41]. Previously reported peptide-based biosensors have served as a platform for the quantitative determination of heavy metal ions [42], proteins [43], proteases [44], kinases [45], nucleic acids [46], antibodies [47], and polysaccharides [48] in practical samples. However, there is a lack of previous studies reporting on the fabrication of a biosensor based on the integration of peptide-induced AIEE of thiolate-protected AuNCs and the usage of a peptide as a recognition element.

The present study introduced four peptide-based sensing methodologies by incorporating two concepts as follows: (1) a peptide triggered the AIEE of glutathione-stabilized gold nanoclusters (GSH-AuNCs) *via* electrostatic attraction between amino groups of the peptide and carboxyl end groups of GSH, and (2) peptide-AuNC aggregates were disassembled by either the complex formation between target analytes and peptides or enzyme-catalyzed hydrolysis of peptide substrates. The recognition events of the presented sensors included the complexation of AG73 peptides with heparin, the hydrolysis of glycine-arginine repeat peptides (GR peptides) by human trypsin, the dephosphorylation of phosphotyrosine- and arginine-containing peptides (pYR peptides) by human alkaline phosphatase (ALP), and the binding of cyclic RGD- and five arginine (R5)-containing peptides (RGDR5 peptides) to integrin receptors. These AIEE-based probes possess high selectivity, comparable sensitivity, and great simplicity. Importantly, these probes were shown to be practically useful for the determination of target analytes in biological fluids and selective imaging of αvβ3 integrin-overexpressing cancer cells.

2. Experimental methods

2.1. Materials and apparatus

All the designed peptide sequences were synthesized from Synpeptide Co. Ltd. (Nanjing, China). Other chemicals are listed in the supplementary material. UV−Vis absorption, fluorescence, and X-ray photoelectron spectroscopy (XPS) spectra were measured on a double-beam spectrophotometer (Cintra 10e; GBC, Victoria, Australia), a Hitachi F-7000 fluorometer (Hitachi, Tokyo, Japan), and a JEOL JAMP-9500F instrument (JEOL, Japan), respectively. A JEM-2100 transmission electron microscopy (TEM; JEOL, Japan) with an accelerating voltage of 200 kV was utilized to collect TEM images. Elemental analyses were carried out using a JEM-2100 TEM coupled with an energy dispersive X-ray spectroscopy (EDS). Zeta potential measurements were performed on Delsa™ nano zeta potential and submicron particle size analyzer (Beckman Coulter Inc., USA). Dynamic light scattering (DLS) spectra were obtained on an N5 submicrometer particle size analyzer (Beckman Coulter, Inc., Fullerton, CA, USA).

Please cite this article as: J.-G. You, W.-L. Tseng, Peptide-induced aggregation of glutathione-capped gold nanoclusters: A new strategy for designing aggregation-induced enhanced emission probes, Analytica Chimica Acta, https://doi.org/10.1016/j.aca.2019.05.069

2.2. Synthesis of GSH-AuNCs and the polypeptide-GSH-AuNC aggregates

An aqueous solution of HAuCl4 (200 mM, 1 mL) was mixed with a solution (9 mL) containing GSH (100 mM, 0.4 mL) and ultrapure water (8.6 mL) under gentle stirring. After 30 min incubation at ambient temperature, a portion of the formed Au(I)-GSH complexes (7 mL) was added to an aqueous solution of GSH (100 mM, 2 mL) [30]. Subsequently, the mixed solutions were heated up to 70 °C for 24 h, generating the GSH-AuNCs. The as-prepared GSH-AuNCs (50 μL, 60 μg mL^{-1}) were prepared in different buffers (50 μL, 100 mM; pH 4.0–10.0). The obtained solutions were incubated with polypeptides (400 μL, 0–25 μg mL^{-1}) at ambient temperature for 10 min, followed by the measurement of their fluorescence spectra at an excitation wavelength of 400 nm.

2.3. Sample preparation

Stock solutions of standards and peptides were prepared in 10 mM HEPES buffer (pH 7.0). GSH-AuNCs were diluted with 10 mM HEPES (pH 7.0). The excitation wavelength was set to 400 nm for the entire experiment. **(a) Sensing of heparin**. GSH-AuNCs (50 μL, 60 μg mL^{-1}) were mixed with AG73 peptides (200 μL, 125 μg mL^{-1}) at ambient temperature. Subsequently, AG73-GSH-AuNC aggregates were incubated with heparin (250 μL, 0–0.2 μM) at ambient temperature for 10 min. The selectivity of the AG73-GSH-AuNC aggregates was examined by replacing heparin with either chondroitin sulfate A or hyaluronic acid. **(b) Sensing of trypsin.** Different concentrations of human trypsin (400 μL, 0–125 nM) catalyzed the hydrolysis of the RG peptides (100 μL, 250 μg mL^{-1}) at 37 °C for 1 h. Then, the digested peptides were incubated with the GSH-AuNCs (50 μL, 60 μg mL^{-1}) at ambient temperature for 10 min. To examine the selectivity of the proposed sensing system, possible interfering proteins were used instead of human trypsin. **(c) Sensing of ALP.** Aqueous solutions of ALP (400 μL, 0–25 U L^{-1}) or other proteins (400 μL, 50 μM) were mixed with the pYR peptides (100 μL, 500 μg mL^{-1}) in 10 mM HEPES buffer (pH 7) at 37 °C for 1 h, followed by incubation with the GSH-AuNCs (50 μL, 60 μg mL^{-1}) at ambient temperature for 10 min. The detailed procedures for the determination of heparin in human plasma, trypsin in human urine, and ALP in human plasma by our proposed probes are described in the supplementary material.

2.4. Cellular imaging

HeLa cells were incubated with the RGDR5-GSH-AuNCs and R5-GSH-AuNCs in DMEM (2 mL) for 2 h in a humidified incubator (5% CO2, 37 °C). Additionally, MCF-7 cells were mixed with the RGDR5-GSH-AuNCs under identical conditions. Then, the cells were rinsed twice with PBS (2 mL 1 × PBS), fixed with paraformaldehyde (2 mL, 4%) for 20 min, and then rinsed twice with PBS (2 mL 1 × PBS). The labeled cells were imaged with a confocal laser scanning microscope (CLSM; LSM 700, Carl Zeiss GmbH, Jena, Germany) equipped with a 63 × oil immersion objective (1.4 N A. and 0.17 mm W.D.) and a 405-nm laser. The luminescence intensity of the peptide-GSH-AuNC aggregates inside the cells was translated across a consecutive range of LUT colors using ImageJ software.

3. Results and discussion

3.1. Polypeptide-induced AIEE of GSH-AuNCs in water

Polyarginine (polyArg)-induced assembly of the GSH-AuNCs was conducted at a neutral pH and ambient temperature (detailed processing methods for the preparation of the polyArg-GSH-AuNC aggregates are included in the experimental section). A neutral pH was used to facilitate an electrostatic attraction between protonated amino groups of polyarginine (pI = 14) and carboxyl end groups (pKa1 = 2 and pKa2 = 3.5) of the GSH-AuNCs (Fig. 1A). After incubating 10 μg mL^{-1} polyArg with 6 μg mL^{-1} GSH-AuNCs in 10 mM (2-hydroxyethyl)-1-piperazine ethanesulfonic acid (HEPES) buffer at pH 7.0, a TEM image showed that the as-synthesized aggregates had a spherical shape with an average particle size of 165 ± 33 nm (n = 20; Fig. 1B). As shown in an enlarged TEM image (Fig. 1C), individual AuNCs with an average particle size of less than 2 nm were observed to be assembled inside the polyArg-GSH-AuNC aggregates. The particle size of these AuNCs inside the aggregates resembled that of free GSH-AuNCs in an aqueous solution. The d-spacing of individual AuNCs was determined to be 0.235 nm, which corresponded to the (111) plane of gold crystals. The elemental composition of the aggregates was analyzed by TEM equipped with EDS. In addition to carbon, oxygen and copper elements from the carbon-coated copper grid, the presence of gold, sulfur, and nitrogen peaks indicated that numerous AuNCs were embedded inside the aggregates (Fig. S1, supplementary material). The particle diameter of the polyArg-GSH-AuNC aggregates measured by DLS was 1.4-fold greater than that measured by TEM (Fig. S2, supplementary material). This difference was due to shrinking of the aggregates during sample drying on the TEM grid. Additionally, the zeta potentials of the GSH-AuNCs and the aggregates were −25 and −10 mV, respectively. Positively charged polyArg can shield the surface charges of the GSH-AuNCs and thus reduce their zeta potential. XPS was used to analyze the change in the valence states of the GSH-AuNCs during the AIEE process. The Au 4f7/2 peaks of the GSH-AuNC and polyArg-GSH-AuNC aggregates were identified to be 83.7 and 83.6 eV, respectively (Fig. 1D and E). The deconvolution of the Au 4f7/2 peak of the GSH-AuNCs resulted in two individual chemical states of Au(0) and Au(I) that were located at 83.5 and 84.0 eV, respectively. The optimal fitting of the XPS data showed that the GSH-AuNCs were composed of 71% Au(0) and 29% Au(I). The same binding energies of Au(0) and Au(I) were used to fit the Au 4f7/2 peak of the aggregates, indicating the presence of 70% Au(0) and 30% Au(I) in the aggregates. Considering that the binding energy of the AuNCs was progressively reduced with increasing cluster size [49], a slight difference in the binding energy between the GSH-AuNC and the polyArg-GSH-AuNC aggregates indicated that the cluster size of the GSH-AuNCs rarely varied during the aggregation process. Additionally, these findings showed that the Au oxidation state of the as-prepared aggregates was nearly similar to that of the GSH-AuNCs. Therefore, the polyArg-based AIEE process scarcely triggered the variation in the Au oxidation in the GSH-AuNCs. Next, we analyzed the luminescence properties of the GSH-AuNCs in the absence and presence of polyArg. The luminescence excitation spectrum of the GSH-AuNCs (dash black curve in Fig. 1F) was remarkably higher than that of the polyArg-GSH-AuNC aggregates (dash red curve in Fig. 1F). Under an excitation wavelength of 400 nm, the GSH-AuNCs emitted low orange luminescence centered at a wavelength of 627 nm (solid black curve in Fig. 1F) with an absolute quantum yield (QY) of 1.2% and a mean luminescence lifetime of 2.2 μs. In contrast to the GSH-AuNCs, the polyArg-GSH-AuNC aggregates showed a 3.5-fold enhancement in luminescence (solid red curve in Fig. 1F), accompanied by an enhanced absolute QY (13%), a blueshifted luminescence peak (8 nm), and a prolonged mean luminescence lifetime (4.6 μs). The intense orange color of the polyArg-GSH-AuNC aggregates was observed under a UV lamp at a wavelength of 365 nm and compared to the GSH-AuNCs (inset in Fig. 1F). The enhancement in the luminescence and QY of the polyArg-GSH-AuNC aggregates was substantially correlated with the AIEE of the GSH-AuNCs. Notably,

Please cite this article as: J.-G. You, W.-L. Tseng, Peptide-induced aggregation of glutathione-capped gold nanoclusters: A new strategy for designing aggregation-induced enhanced emission probes, Analytica Chimica Acta, https://doi.org/10.1016/j.aca.2019.05.069

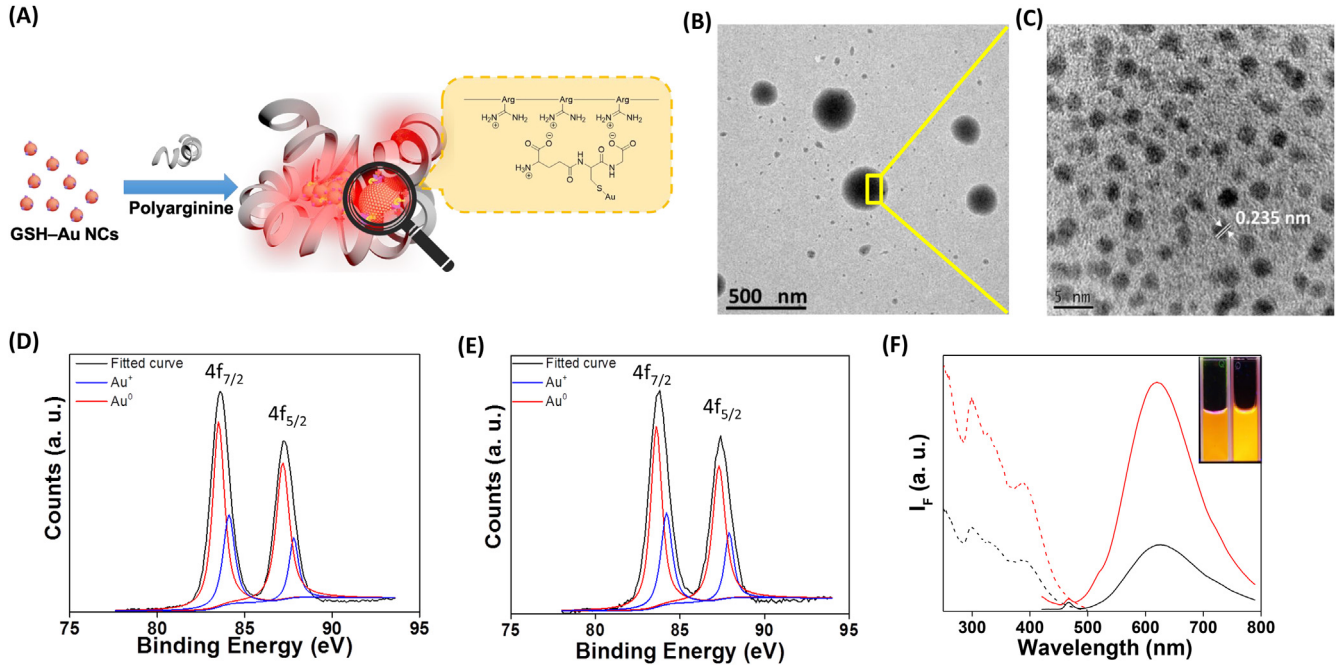

Fig. 1. PolyArg-induced AIEE of the GSH-AuNCs. (A) A schematic of polyArg-triggered aggregation of the GSH-AuNCs. (B) A TEM image of the polyArg-GSH-AuNC aggregates. (C) An enlarged section of the TEM image showing a portion of the polyArg-GSH-AuNC aggregates. (D) XPS spectrum of the GSH-AuNCs. (E) XPS spectrum of the polyArg-GSH-AuNC aggregates. (F) Luminescence excitation spectra of the GSH-AuNCs (dash black curve) and the polyArg-GSH-AuNC aggregates (dash red curve) and luminescence emission spectra of the GSH-AuNCs (solid black curve) and the polyArg-GSH-AuNC aggregates (solid red curve). Inset in (F): images of the GSH-AuNCs (left) and the polyArg-GSH-AuNC aggregates (right). The images were obtained under UV light at a wavelength of 365 nm. (For interpretation of the references to color in this figure legend, the reader is referred to the Web version of this article.)

the assembly of the GSH-AuNCs was capable of increasing the inter and intramolecular aurophilic attractions between the two Au(I) atoms and impeding the intramolecular rotation/vibration of GSH [50]. These contributions caused the assembled GSH-AuNCs to emit bright luminescence with a long luminescence lifetime [30]. Moreover, nanocluster aggregation-induced blueshift in the maximum luminescence suggested that the intermolecular aurophilic attraction between the adjoining AuNCs governed the polyArg-mediated aggregation of the GSH-AuNCs, leading to an extension in the average distance between the two Au(I) atoms [51].

We explored the factors that influence the polyArg-triggered AIEE of the GSH-AuNCs. The AIEE efficiency of the GSH-AuNCs was evaluated by analyzing their luminescence intensity at a wavelength of 619 nm. In contrast to neutral polythreonine (5–15 kDa) and anionic polyglutamic acid (15–50 kDa), cationic polyArg (15–70 kDa) efficiently promoted the AIEE of the GSH-AuNCs (Fig. S3, supplementary material). Collectively, this result indicated that the electrostatic attraction between the cationic polypeptide and anionic GSH is a key factor in causing the formation of AIEE-type luminescent aggregates, and this behavior was consistent with previous findings showing poly(allylamine hydrochloride)- and chitosan-induced AIE of the GSH-AuNCs [25,26]. The luminescence intensity of the polyArg-GSH-AuNC aggregates progressively increased in the pH range of 2.0–4.0 and leveled off above pH 4.0 (Fig. S4, supplementary material). Considering that the smallest pKa value of GSH is 2.0, the GSH-AuNCs are suggested to have negative charges at neutral and alkaline pH values. Therefore, the GSH-AuNCs could have strong electrostatic attraction with polyArg above pH 4.0, resulting in high AIEE efficiency. As shown in Fig. S5 (supplementary material), the luminescence of the polyArg-GSH-AuNC aggregates gradually intensified with increasing polyArg concentration and reached a saturation level at 10 μg mL^{-1} polyArg. Accordingly, the optimal ratio of polyArg to GSH-AuNCs for preparing the bright aggregates was determined to be 5:3. Furthermore, we focused on the investigation of the stability of the polyArg-GSH-AuNC aggregates under varied conditions. The luminescence intensity (619 nm) of the polyArg-GSH-AuNC aggregates remained nearly unchanged when suspended in 0–300 mM NaCl, 10 mM GSH, and 1 mg mL^{-1} human trypsin (Fig. S6, supplementary material). In addition to HEPES buffer (pH 7.0), polyArg was observed to induce the AIEE of the GSH-AuNCs in phosphate, Tris-HCl, citrate, acetate, and 3-(N-morpholino) propanesulfonic acid (MOPS) buffers (pH 7.0; Fig. S7, supplementary material). These observations indicate that the polypeptide-GSH-AuNC aggregates may have considerable potential for use in the imaging and sensing of target analytes in practical samples.

3.2. Fabrication of AIEE-Active sensors

The integration of (1) cationic polypeptide-induced AIEE of the GSH-AuNCs and (2) the use of a polypeptide as a recognition element allows the development of a series of optical sensors, which demonstrate the broader applicability of the concepts mentioned above. Table S1 (supplementary material) lists the sequences of the AG73, GR, pYR, and RGDR5 peptides that were used in the development of heparin-, trypsin-, ALP-, and integrin receptor-responsive biosensors, respectively. To assure whether the above peptides could promote the assembly of the GSH-AuNCs and then enhance their luminescence, we compared the GSH-AuNCs with the aggregates in terms of morphology, zeta potential, and luminescence properties. As summarized in Table 1, TEM, DLS, XPS, and luminescence studies showed that the incubation of the GSH-AuNCs with cationic peptides, including AG73, GR, dephosphorylated pYR, and RGDR5, all resulted in the production of large-sized aggregates (Figs. S8 and S9, supplementary material). Compared to

Please cite this article as: J.-G. You, W.-L. Tseng, Peptide-induced aggregation of glutathione-capped gold nanoclusters: A new strategy for designing aggregation-induced enhanced emission probes, Analytica Chimica Acta, https://doi.org/10.1016/j.aca.2019.05.069

Table 1
The physical and optical properties of the GSH-AuNCs and the peptide-GSH-AuNC aggregates.

Composites	QY (%)	λ_{em} (nm)	Zeta Potential (mV)	Diameter by DLS (nm)	Diameter by TEM (nm)	Lifetime (μs)	Au(0): Au(I)
GSH-AuNCs	1.2	627	−25	N.A.	1.7 ± 0.1	2.2	71:29
PolyArg, GSH-AuNCs	13	619	−10	227	165 ± 33	4.6	70:30
AG73, GSH-AuNCs	11	619	−16	199	127 ± 32	3.8	70:30
GR, GSH-AuNCs	10	612	−14	210	132 ± 31	4.3	70:30
YR,[a] GSH-AuNCs	15	614	−13	197	118 ± 17	4.8	N.D.[b]
$RGDR_5$, GSH-AuNCs	12	616	−13	207	149 ± 24	4.2	70:30
R_5, GSH-AuNCs	12	614	−12	204	142 ± 20	4.3	N.D.[b]

[a] YR, dephosphorylated pYR.
[b] N.D., not detected.

the GSH-AuNCs, the four aggregates that were formed all possessed an enhanced QY, increased luminescence lifetime, reduced zeta potential, unchanged ratio of Au(0) to Au(I) (Fig. S10, supplementary material), and blueshifted luminescence peak (Fig. S11, supplementary material). The sensitivity, selectivity, and practical application of four AIEE-active sensors were explored in the subsequent study. For the first example, we created a turn-off assay for luminescent detection of heparin through AG73 peptide-triggered AIEE of the GSH-AuNCs. Notably, the high-pI (12.4) AG73 peptide has been shown to exhibit specific binding affinity to heparin [48]. Fig. 2A shows the complete mechanism of the probe for heparin sensing. The electrostatic attraction between the AG73 peptides and the GSH-AuNCs promoted the assembly of the GSH-AuNCs. The formed AG73-GSH-AuNC aggregates emitted intense luminescence due to the AIEE process. Because heparin was present in the solution, the complexation of heparin with the AG73 peptide activated the disassembly of the AG73-GSH-AuNC aggregates. As a result, the disassembled aggregates showed weak luminescence. In other words, heparin switched off the luminescence of the AG73-GSH-AuNC aggregates. Evidently, TEM images showed the disassembly of the AG73-GSH-AuNC aggregates in the presence of heparin (Fig. S12, supplementary material). As shown in Fig. 2B, the luminescence of the AG73-GSH-AuNC aggregates gradually decreased with an increase in the heparin concentration. By plotting the *(IF0 − IF)/IF0* value against the heparin concentration, a linear calibration curve was established for heparin for concentrations ranging from 8 to 80 nM (inset in Fig. 2B). *IF0* and *IF* are the maximal luminescent intensities (616 nm) of the AG73-GSH-AuNC aggregates before and after adding the tested analytes, respectively. The limit of detection (LOD) of heparin, defined as a signal-to-noise

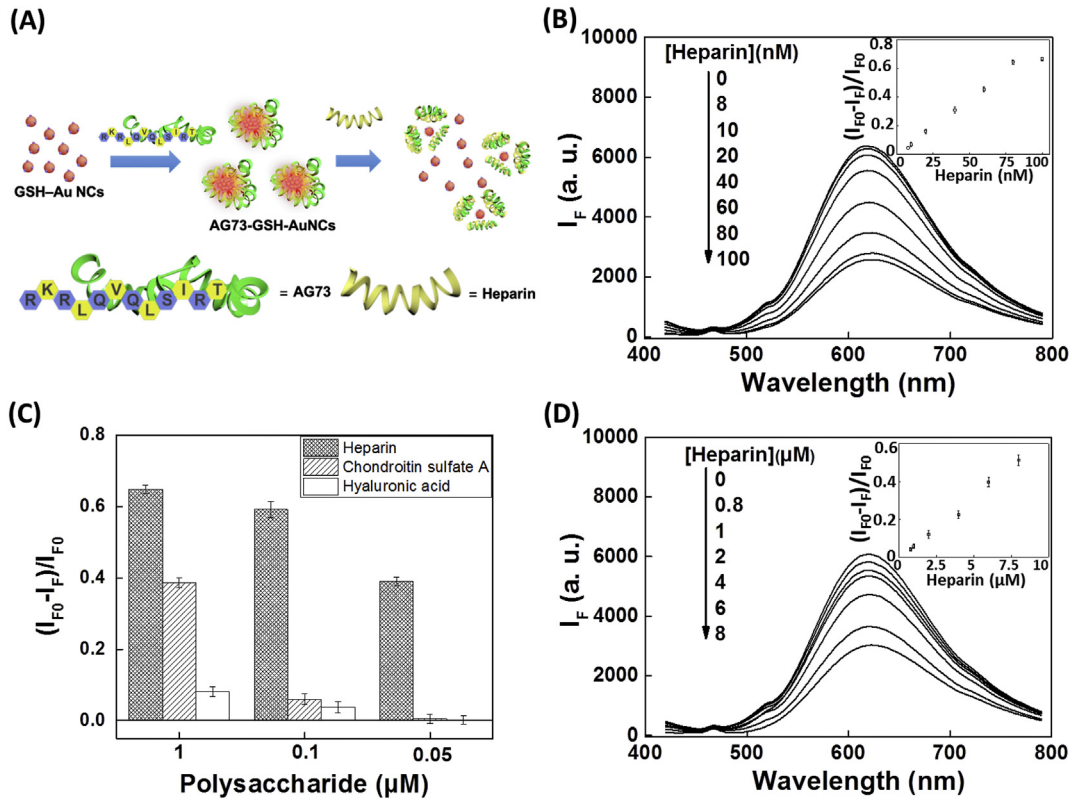

Fig. 2. Turn-off sensing of heparin. (A) Selective detection of heparin based on the combination of the AG73 peptide-induced AIEE of the GSH-AuNCs and heparin-triggered disassembly of the AG73-GSH-AuNC aggregates. (B) Luminescence spectra of the AG73-GSH-AuNC aggregates in the presence of increasing concentrations of heparin. Inset: A plot of the (IF0 − IF)/IF0 value *versus* the heparin concentration. (C) The (IF0 − IF)/IF0 value of the AG73-GSH-AuNC aggregates after the addition of 0.05−1 μM heparin, chondroitin sulfate A, and hyaluronic acid. (D) Fluorescent spectral response obtained from the addition of heparin-spiked plasma to a solution of the AG73-GSH-AuNC aggregates. Inset: A plot of the (IF0 − IF)/IF0 value *versus* the spiked concentration of heparin in human plasma. (B, C, D) The AG73-GSH-AuNC aggregates were incubated with heparin in 10 mM HEPES (pH 7.0) for 10 min. The error bars represent standard deviations based on three independent measurements.

Please cite this article as: J.-G. You, W.-L. Tseng, Peptide-induced aggregation of glutathione-capped gold nanoclusters: A new strategy for designing aggregation-induced enhanced emission probes, Analytica Chimica Acta, https://doi.org/10.1016/j.aca.2019.05.069

ratio of 3, was estimated to be 3 nM. Although the sensitivity of the probe was only comparable to that of previously reported sensors (Table S2, supplementary material), it was sufficiently sensitive for monitoring plasma heparin levels during cardiovascular surgery (17–67 μM) and during postoperative care and long-term treatment (1.7–10 μM) [52]. Subsequently, this study assessed the selectivity of the AG73-GSH-AuNC aggregates toward heparin over possible interfering compounds, including chondroitin sulfate, hyaluronic acid, low-pI proteins, negatively charged biomolecules, and anions (Fig. 2C; Fig. S13, supplementary material). Only the addition of heparin generated a remarkably high *(IF0 − IF)/IF0* value, indicating that the probe was selectively responsive to heparin. However, the probe exhibited a significant response in the presence of high concentration of chondroitin sulfate since chondroitin sulfate are also highly sulfated (0.95 sulfate groups per disaccharide unit) [53]. Samples of human plasma were spiked with different quantities of standard heparin prior to sample pretreatment. Because the spiked concentration of heparin varied from 0.8 to 8 μM, we observed a progressive reduction in the luminescence of the probe and a linear relationship between the *(IF0 − IF)/IF0* value and the added heparin concentration (Fig. 2D). A method LOD of heparin in this assay was determined to be 300 nM.

For the second example, polypeptide-induced AIEE of the GSH-AuNCs was used for luminescence turn-off and turn-on sensing of human trypsin and ALP, respectively. As shown in Fig. 3A, the designed GR peptide consisting of an arginine and glycine repeat sequence contributed a net positive charge at a neutral pH, allowing the AIEE of the GSH-AuNCs. Human trypsin specifically recognized and cleaved the GR peptide at the carboxyl ends of arginine and lysine [54]. The short peptide had few positive charges, leading to an inefficient AIEE of the GSH-AuNCs. TEM images confirmed that the digested GR peptide rarely promoted the aggregation of the GSH-AuNCs (Fig. S14, supplementary material). Because different concentrations (1–100 nM) of human trypsin were incubated with a fixed concentration of the GR peptide in 10 mM HEPES (pH 7.0), the luminescence of the GR-GSH-AuNC aggregates progressively decreased with increasing concentrations of human trypsin (Fig. 3B). The linear relationship between the *(IF1 − IF2)/IF1* value and the trypsin concentration was observed in the range of 1–10 nM (inset in Fig. 3B). The variables *IF1* and *IF2* represent the luminescence intensity (612 nm) of the GR-GSH-AuNC aggregates in the disappearance and appearance of human trypsin, respectively. This probe allowed the sensing of human trypsin with an LOD of 0.3 nM, which was superior to the LOD values obtained from previously reported probes (Table S3, supplementary material). Fig. 3C shows that the *(IF1 − IF2)/IF1* value was remarkably high in the presence of human trypsin, indicating that the GR-GSH-AuNC aggregates exhibited distinctive selectivity toward human trypsin over several potentially interfering proteins. To confirm the capability of the GR-GSH-AuNC aggregates to detect human trypsin in practical samples, human urine samples were mixed with a series of known concentrations of human trypsin. As shown in Fig. 3D, the

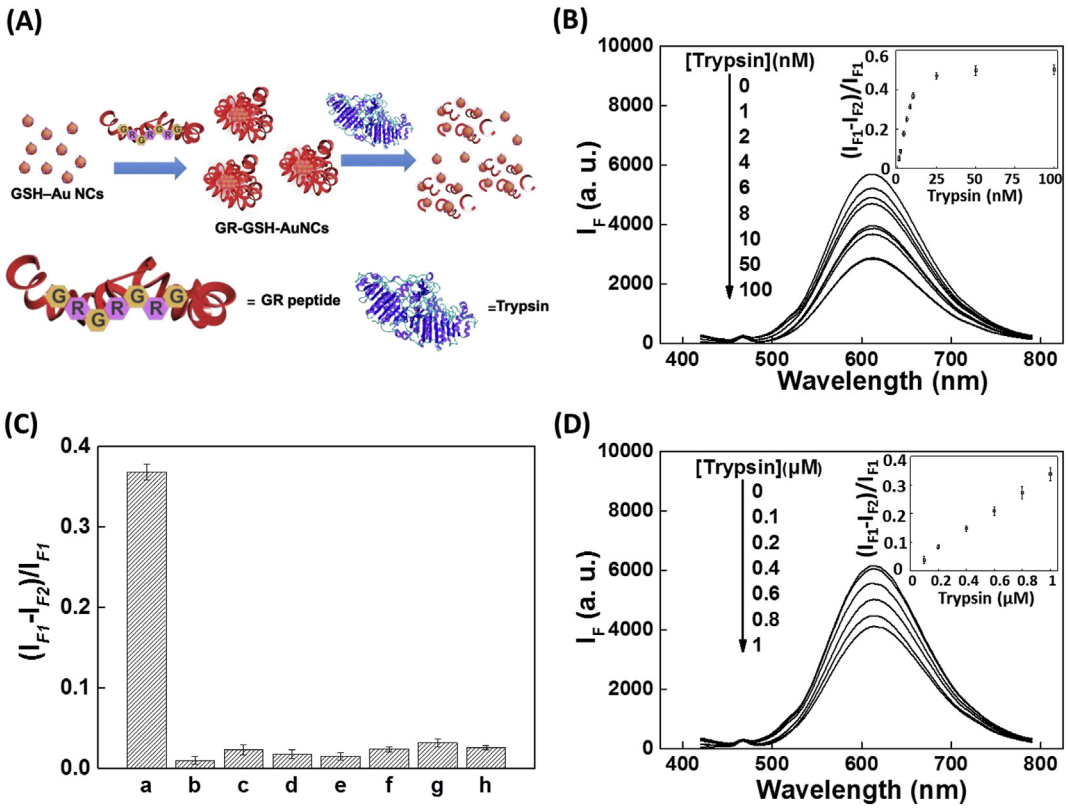

Fig. 3. Turn-off sensing of human trypsin. (A) The integration of trypsin-mediated hydrolysis of the GR peptide and the GR peptide-induced AIEE of the GSH-AuNCs for probing human trypsin. (B) Luminescence spectra of the GSH-AuNCs obtained after the addition of a mixture of 50 μg mL^{-1} GR peptide and 0–100 nM human trypsin. Inset: A plot of the (IF1 − IF2)/IF1 value *versus* the trypsin concentration. (C) The (IF1 − IF2)/IF1 value of the GSH-AuNCs obtained after the addition of a mixture of 50 μg mL^{-1} GR peptide and protein. Protein: (a) 10 nM human trypsin, (b) 10 U L^{-1} ALP, (c) 10 nM bovine serum albumin, (d) 10 nM human serum albumin, (e) 10 nM lysozyme, (f) 10 nM glucose oxidase, (g) 10 nM pepsin, and (h) 10 nM myoglobin. (D) Luminescent spectral response measured from the addition of trypsin-spiked urine to a solution of the GR peptide, followed by the incubation of the GSH-AuNCs. Inset: A plot of the (IF1 − IF2)/IF1 value *versus* the spiked concentration of trypsin in human urine. (B, C, D) Various concentrations of human trypsin reacted with the GR peptide in 10 mM HEPES (pH 7.0) at 37 °C for 1 h and were then incubated with the GSH-AuNCs for 10 min. The error bars represent standard deviations based on three independent measurements.

Please cite this article as: J.-G. You, W.-L. Tseng, Peptide-induced aggregation of glutathione-capped gold nanoclusters: A new strategy for designing aggregation-induced enhanced emission probes, Analytica Chimica Acta, https://doi.org/10.1016/j.aca.2019.05.069

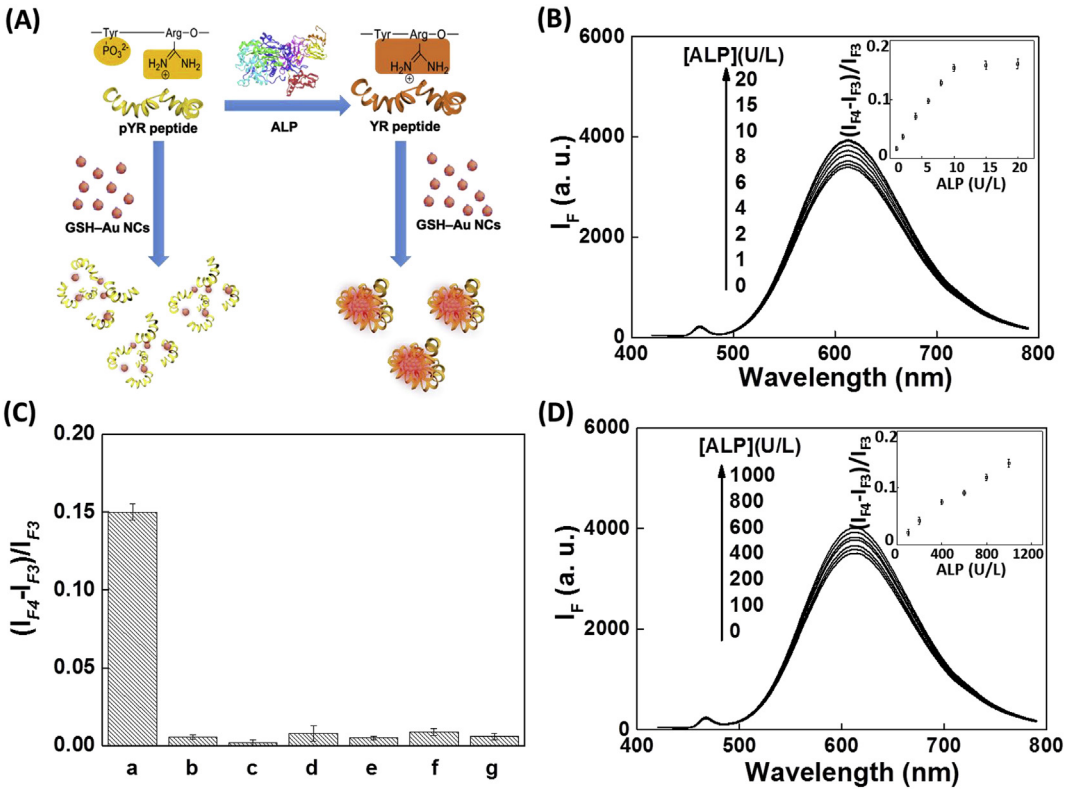

Fig. 4. Turn-on sensing of human ALP. (A) Specific detection of human ALP through ALP-mediated dephosphorylation of the pYR peptide paired with dephosphorylated pYR peptide-triggered AIEE of the GSH-AuNCs. (B) Fluorescence spectra of the GSH-AuNCs obtained after the addition of a mixture of 50 μg mL^{-1} pYR peptide and 0–20 U L^{-1} human ALP. Inset: A plot of the (IF4 − IF3)/IF3 value *versus* the ALP concentration. (C) The (IF4 − IF3)/IF3 value of the GSH-AuNCs obtained after the addition of a mixture of the pYR peptide and protein. Protein: (a) 10 U L^{-1} ALP, (b) 50 μM bovine myoglobin, (c) 50 μM lysozyme, (d) 50 μM human serum albumin, (e) 50 μM bovine cytochrome C, (f) 50 μM bovine serum albumin, and (g) 50 μM pepsin. (D) Fluorescent spectral response measured from the addition of ALP-spiked plasma to a solution of the pYR peptide, followed by the incubation of the GSH-AuNCs. Inset: A plot of the (IF4 − IF3)/IF3 value *versus* the spiked concentration of ALP in human urine. (B, C, D) Various concentrations of human ALP reacted with the pYR peptide in 10 mM HEPES (pH 7.0) at 37 °C for 1 h and were then incubated with the GSH-AuNCs for 10 min. The error bars represent standard deviations based on three independent measurements.

luminescence of the GR-GSH-AuNC aggregates incrementally decreased with increasing trypsin concentrations in human urine, generating a linear calibration curve for the quantification of 0.1–1 μM urinary trypsin with a method LOD of 30 nM (0.72 μg mL^{-1}). We suggest that the proposed system, consisting of trypsin-catalyzed hydrolysis of the GR peptide and the GR peptide-induced AIEE of the GSH-AuNCs, is sensitive enough to monitor the level of urinary trypsin (84.4 μg mL^{-1}, 3.6 μM) in pancreas transplant patients [55]. For sensing ALP, the pYR peptide was used in place of the GR peptide under the same sensing conditions. The synthesized pYR peptide consisted of two phosphorylated tyrosines and six arginines (Fig. 4A). The negatively charged phosphate group on the side chain of tyrosine prohibited the electrostatic attraction between the negatively charged carboxyl ends of the

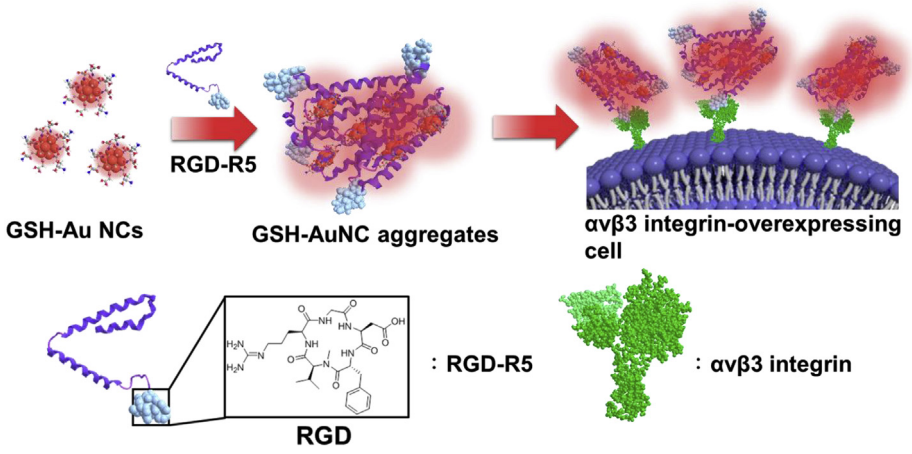

Fig. 5. A schematic of the preparation of the RGDR5-GSH-AuNC aggregates and their specificity and enhanced uptake by αvβ3 integrin-positive cells.

Please cite this article as: J.-G. You, W.-L. Tseng, Peptide-induced aggregation of glutathione-capped gold nanoclusters: A new strategy for designing aggregation-induced enhanced emission probes, Analytica Chimica Acta, https://doi.org/10.1016/j.aca.2019.05.069

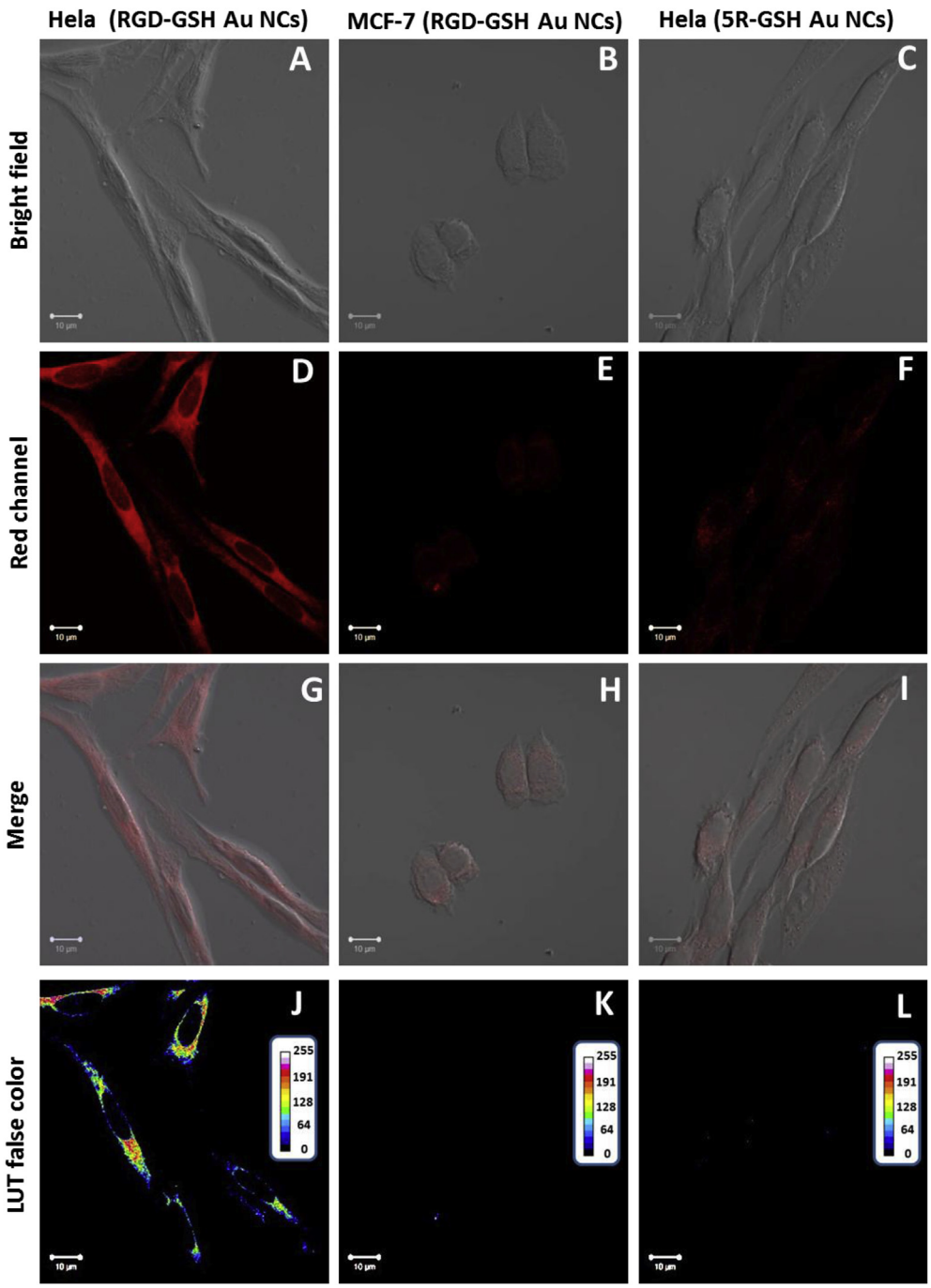

Fig. 6. Intracellular imaging of the RGDR5-GSH-AuNC aggregates and the R5-GSH-AuNC aggregates in cancer cells. (A, B, C) Bright-field, (D, E, F) CLSM, and (J, K, L) luminescence intensity images obtained from the incubation of (A, D, J) the RGDR5-GSH-AuNC aggregates with HeLa cells, (B, E, K) the RGDR5-GSH-AuNC aggregates with MCF-7 cells, and (C, F, L) the R5-GSH-AuNC aggregates with HeLa cells. (G), (H), and (I) show merged images of (A) and (D), (B) and (E), as well as (C) and (F), respectively. The LUT false color represents the intensity of the luminescence signal. The concentrations of the RGDR5-GSH-AuNC aggregates and the R5-GSH-AuNC aggregates were 250 and 250 μg mL^{-1}, respectively. The scale bar indicates 10 μm. (For interpretation of the references to color in this figure legend, the reader is referred to the Web version of this article.)

GSH-AuNCs and the positively charged guanidine group of arginine. In other words, the GSH-AuNCs remained dispersed upon the addition of the pYR peptide. After ALP eliminated phosphate groups from the pYR peptide, the resulting dephosphorylated peptide with a net positive charge was capable of promoting the AIEE of the GSH-AuNCs. Thus, the AIEE efficiency of the GSH-AuNCs heavily relied on the concentration of the dephosphorylated peptides. After different concentrations of ALP catalyzed the hydrolysis of the pYR peptide at a neutral pH, the resultant products were incubated with the GSH-AuNCs. Fig. 4B shows that the luminescence of the GSH-AuNCs was gradually enhanced with increasing concentrations of ALP. Plotting of the $(IF4 - IF3)/IF3$ value versus the ALP concentration generated a linear calibration curve over the concentration range of 1–10 U L^{-1} (inset in Fig. 4B). *IF3* and *IF4* refer to the luminescence intensities of the GSH-AuNCs at a wavelength of 614 nm obtained from incubation without and with the addition of ALP, respectively. The LOD of ALP that was analyzed by the proposed strategy was determined to be 0.3 U L^{-1}. We suggest that the sensitivity of the proposed

Please cite this article as: J.-G. You, W.-L. Tseng, Peptide-induced aggregation of glutathione-capped gold nanoclusters: A new strategy for designing aggregation-induced enhanced emission probes, Analytica Chimica Acta, https://doi.org/10.1016/j.aca.2019.05.069

strategy is comparable to those of previously reported probes (Table S4, supplementary material). As shown in Fig. 4C, ALP-mediated hydrolysis of the pYR peptide combined with cationic peptide-induced AIEE of the GSH-AuNCs exhibited exceptional selectivity toward ALP over the other proteins. The human plasma samples were mixed with the pYR peptide and then spiked with different known concentrations of ALP. As shown in Fig. 4D, the luminescence of the GSH-AuNCs gradually intensified with increasing spiked concentrations of ALP in the human plasma samples. The level of ALP in the human plasma samples was estimated to be 108 U L^{-1} (n = 3; inset in Fig. 4D) according to the standard addition method. This value was within the accepted normal range (46–190 U L^{-1}) of ALP in human plasma [56].

3.3. AIEE-based imaging probes

Integrins, a family of cell surface receptors, are composed of one α-subunit and one β-subunit [57]. They primarily mediate cell-extracellular matrix adhesion and cell-cell interactions [58]. Since the tripeptide RGD motif has been shown to provide broad binding specificity toward integrin-overexpressing cancer cells, numerous studies have focused on the development of RGD-functionalized nanoprobes for biomedical applications [59]. The preparation of the RGDR5-GSH-AuNC aggregates is shown in a schematic in Fig. 5. The RGDR5 peptide consisting of an AIEE-active sequence (five arginine repeats) and a cyclic RGD sequence was utilized to trigger the AIEE of the GSH-AuNCs at a neutral pH. A standard 3-(4,5-dimethylthiazol-2-yl)-2,5-diphenyltetrazolium bromide (MTT) assay showed that the viability of HeLa cells all remained above 90% in the presence of 250, 125, and 62.5 μg mL^{-1} of the RGDR5-GSH-AuNC aggregates for 24 h, indicating good biocompatibility of the RGDR5-GSH-AuNC aggregates (Fig. S15, supplementary material). To demonstrate their specificity and enhanced uptake by αvβ3 integrin-positive cells, the RGDG-GSH-AuNC aggregates were taken up by MCF-7 cells (low αvβ3 integrin expression) and HeLa cells (high αvβ3 integrin expression) for 2 h [60]. For control experiments, we treated HeLa cells with the same concentration of the RGD-free aggregates, which were formed by mixing an R5-containing peptide and the GSH-AuNCs at a neutral pH. Notably, the quantum yield and particle size of the RGDR5-GSH-AuNC aggregates were similar to those of the R5-GSH-AuNC aggregates (Table 1). The labeled cells mentioned above were imaged using CLSM under the same laser power and exposure time. Fig. 6A, B, and C show bright-field images of HeLa cells treated with the RGDR5-GSH-AuNC aggregates, MCF-7 cells labeled with the RGDR5-GSH-AuNC aggregates, and HeLa cells cultured with the R5-GSH-AuNC aggregates, respectively. The CLSM images show that the luminescence of RGDR5-GSH-AuNC aggregates inside HeLa cells (Fig. 6D) was extraordinarily bright in comparison to that of the RGDR5-GSH-AuNC aggregates inside the MCF-7 cells (Fig. 6E) and that of the R5-GSH-AuNC aggregates inside HeLa cells (Fig. 6F). The corresponding pseudocolor images show the luminescence intensity of the peptide-AuNC aggregates inside the cancer cells (Fig. 6J, K, and L), further confirming the results observed by CLSM imaging. The merged images show that the red luminescence of the RGDR5-GSH-AuNC aggregates was localized in the cell cytoplasm (Fig. 6G, H, and I). Likewise, Ding et al. modified BSA-stabilized AuNCs with cyclic RGD and used them for probing the αvβ3 integrin on the surface of HeLa cells [61]. They demonstrated that HeLa cells could efficiently internalize cyclic RGD-modified AuNCs via the endocytosis process. Liang et al. prepared cyclic RGD-capped AuNCs via direct mixing of HAuCl4 and an RGD-containing peptide at an alkaline pH and used them for selectively imaging HeLa cells. The luminescence of RGD-modified AuNCs was observed to be localized inside the cells. According to previously reported studies and our findings, we proposed a possible mechanism associated with the recognition of HeLa cells by RGDR5-GSH-AuNC aggregates. The cyclic RGD on the surface of the aggregates retains sufficient activity to bind αvβ3 integrin-overexpressed HeLa cells, facilitating the RGDR5-GSH-AuNC aggregates to enter the cells via receptor-mediated endocytosis [61]. As a result, the RGDR5-GSH-AuNC aggregates were uniformly distributed in the cell cytoplasm. In contrast, the RGDR5-GSH-AuNC aggregates weakly bind the MCF-7 cells that express low levels of αvβ3 integrin, resulting in low red luminescence inside the cells. Since the R5-GSH-AuNC aggregates did not contain cyclic RGD, they were incapable of interacting with HeLa cells through the recognition of the αvβ3 integrin. The endocytosis of the R5-GSH-AuNC aggregates by HeLa cells resulted in weak red luminescence inside the cells. We suggest that the RGDR5-GSH-AuNC aggregates could serve as a promising probe for luminescence imaging of αvβ3 integrin-overexpressing cancer cells.

4. Conclusions

The present study demonstrated that cationic peptides promoted efficient AIEE of the GSH-AuNCs through electrostatic attraction between negatively charged carboxylic groups of the GSH-AuNCs and positively charged amino groups of the peptides. Compared to the GSH-AuNCs, the peptide-GSH-AuNC aggregates generally exhibited improved QYs, prolonged luminescence lifetime, and a blueshifted luminescence maximum. The versatility of peptide-based biosensor design was exemplified by using four different cationic peptides (including AG73, GR, pYR, and RGDR5) to stimulate the AIEE of the GSH-AuNCs. The designed peptides included AG73, RG, pYR, and RGDR5, which were shown to be selectively responsive to heparin, trypsin, ALP, and αvβ3 integrin receptors, respectively. Importantly, the proposed biosensors were practically used for quantitative determination of heparin, human trypsin, and human ALP in human fluids, as well as for luminescent sensing of αvβ3 integrin-overexpressed cancer cells. Considering that peptides have been identified as recognition elements to bind proteins, nucleic acids, metal ions, and bacteria [62,63], we suggest that this study provides a new strategy for the fabrication of novel peptide-based biosensors based on the mechanism of peptide-induced AIEE of the GSH-AuNCs.

Notes

The authors declare no competing financial interest.

Conflict of interest

To the best of our knowledge, the named authors have no conflict of interest, financial or otherwise.

Acknowledgements

We would like to appreciate the funding support from the Ministry of Science and Technology (MOST107-2113-M-110 -013 -MY3).

Appendix A. Supplementary data

Supplementary data to this article can be found online at https://doi.org/10.1016/j.aca.2019.05.069.

References

[1] G. Li, R. Jin, Atomically precise gold nanoclusters as new model catalysts, Acc.

Chem. Res. 46 (2013) 1749–1758.
[2] L.-Y. Chen, C.-W. Wang, Z. Yuan, H.-T. Chang, Fluorescent gold nanoclusters: recent advances in sensing and imaging, Anal. Chem. 87 (2015) 216–229.
[3] T. Yokoyama, N. Hirata, H. Tsunoyama, Y. Negishi, A. Nakajima, Characterization of floating-gate memory device with thiolate-protected gold and gold-palladium nanoclusters, AIP Adv. 8 (2018) 065002.
[4] Y. Tao, M. Li, J. Ren, X. Qu, Metal nanoclusters: novel probes for diagnostic and therapeutic applications, Chem. Soc. Rev. 44 (2015) 8636–8663.
[5] H. Liao, G. Liu, Y. Liu, R. Li, W. Fu, L. Hu, Aggregation-induced accelerating peroxidase-like activity of gold nanoclusters and their applications for colorimetric Pb2+ detection, Chem. Comm. 53 (2017) 10160–10163.
[6] L. Hu, H. Liao, L. Feng, M. Wang, W. Fu, Accelerating the peroxidase-like activity of gold nanoclusters at neutral pH for colorimetric detection of heparin and heparinase activity, Anal. Chem. 90 (2018) 6247–6252.
[7] P.D. Jadzinsky, G. Calero, C.J. Ackerson, D.A. Bushnell, R.D. Kornberg, Structure of a thiol monolayer-protected gold nanoparticle at 1.1 Å resolution, Science 318 (2007) 430–433.
[8] R. Jin, Quantum sized, thiolate-protected gold nanoclusters, Nanoscale 2 (2010) 343–362.
[9] R.W. Murray, Nanoelectrochemistry: metal nanoparticles, nanoelectrodes, and nanopores, Chem. Rev. 108 (2008) 2688–2720.
[10] L. Shang, S. Dong, G.U. Nienhaus, Ultra-small fluorescent metal nanoclusters: synthesis and biological applications, Nano Today 6 (2011) 401–418.
[11] Z. Wu, R. Jin, On the ligand's role in the fluorescence of gold nanoclusters, Nano Lett. 10 (2010) 2568–2573.
[12] L. Polavarapu, M. Manna, Q.-H. Xu, Biocompatible glutathione capped gold clusters as one- and two-photon excitation fluorescence contrast agents for live cells imaging, Nanoscale 3 (2011) 429–434.
[13] S. Chattoraj, M.A. Amin, S. Mohapatra, S. Ghosh, K. Bhattacharyya, Cancer cell imaging using in situ generated gold nanoclusters, ChemPhysChem 17 (2016) 61–68.
[14] Z. Yuan, M. Peng, L. Shi, Y. Du, N. Cai, Y. He, H.-T. Chang, E.S. Yeung, Disassembly mediated fluorescence recovery of gold nanodots for selective sulfide sensing, Nanoscale 5 (2013) 4683–4686.
[15] C. Zong, L.R. Zheng, W. He, X. Ren, C. Jiang, L. Lu, In situ formation of phosphorescent molecular gold(I) cluster in a macroporous polymer film to achieve colorimetric cyanide sensing, Anal. Chem. 86 (2014) 1687–1692.
[16] P.-H. Li, J.-Y. Lin, C.-T. Chen, W.-R. Ciou, P.-H. Chan, L. Luo, H.-Y. Hsu, E.W.-G. Diau, Y.-C. Chen, Using gold nanoclusters as selective luminescent probes for phosphate-containing metabolites, Anal. Chem. 84 (2012) 5484–5488.
[17] L. Hu, S. Han, S. Parveen, Y. Yuan, L. Zhang, G. Xu, Highly sensitive fluorescent detection of trypsin based on BSA-stabilized gold nanoclusters, Biosens. Bioelectron. 32 (2012) 297–299.
[18] L. Zhang, J. Zhu, Z. Zhou, S. Guo, J. Li, S. Dong, E. Wang, A new approach to light up DNA/Ag nanocluster-based beacons for bioanalysis, Chem. Sci. 4 (2013) 4004–4010.
[19] C.-Y. Ke, Y.-T. Wu, W.-L. Tseng, Fluorescein-5-isothiocyanate-conjugated protein-directed synthesis of gold nanoclusters for fluorescent ratiometric sensing of an enzyme–substrate system, Biosens. Bioelectron. 69 (2015) 46–53.
[20] H.-C. Chang, Y.-F. Chang, N.-C. Fan, J.-a.A. Ho, Facile preparation of high-quantum-yield gold nanoclusters: application to probing mercuric ions and biothiols, ACS Appl. Mater. Interfaces 6 (2014) 18824–18831.
[21] X. Le Guével, V. Trouillet, C. Spies, K. Li, T. Laaksonen, D. Auerbach, G. Jung, M. Schneider, High photostability and enhanced fluorescence of gold nanoclusters by silver doping, Nanoscale 4 (2012) 7624–7631.
[22] X. Wu, C. Li, S. Liao, L. Li, T. Wang, Z. Su, C. Wang, J. Zhao, C. Sui, J. Lin, Silica-encapsulated Gd3+-aggregated gold nanoclusters for in vitro and in vivo multimodal cancer imaging, Chem. Eur. J. 20 (2014) 8876–8882.
[23] L. Ji, Y. Guo, S. Hong, Z. Wang, K. Wang, X. Chen, J. Zhang, J. Hu, R. Pei, Label-free detection of Pb2+ based on aggregation-induced emission enhancement of Au-nanoclusters, RSC Adv. 5 (2015) 36582–36586.
[24] X. Lu, T. Wang, T. Shu, X. Qu, X. Zhang, F. Liang, L. Su, Combination of chemical etching of gold nanoclusters with aggregation-induced emission for preparation of new phosphors for the development of UV-driven phosphor-converted white light-emitting diodes, J. Mater. Chem. C 4 (2016) 11482–11487.
[25] A. Yahia-Ammar, D. Sierra, F. Mérola, N. Hildebrandt, X. Le Guével, Self-assembled gold nanoclusters for bright fluorescence imaging and enhanced drug delivery, ACS Nano 10 (2016) 2591–2599.
[26] N. Goswami, F. Lin, Y. Liu, D.T. Leong, J. Xie, Highly luminescent thiolated gold nanoclusters impregnated in nanogel, Chem. Mater. 28 (2016) 4009–4016.
[27] X. Xin, Y. Gao, Q. Zhang, Z. Wang, D. Sun, S. Yuan, H. Xia, Realizing enhanced luminescence of silver nanocluster–peptide soft hydrogels by PEI reinforcement, Soft Matter 14 (2018) 8352–8360.
[28] Z. Luo, X. Yuan, Y. Yu, Q. Zhang, D.T. Leong, J.Y. Lee, J. Xie, From aggregation-induced emission of Au(I)–thiolate complexes to ultrabright Au(0)@Au(I)–thiolate core–shell nanoclusters, J. Am. Chem. Soc. 134 (2012) 16662–16670.
[29] B. Li, X. Wang, X. Shen, W. Zhu, L. Xu, X. Zhou, Aggregation-induced emission from gold nanoclusters for use as a luminescence-enhanced nanosensor to detect trace amounts of silver ions, J. Colloid Interface Sci. 467 (2016) 90–96.
[30] J.-G. You, C.-Y. Lu, A.S. Krishna Kumar, W.-L. Tseng, Cerium(III)-directed assembly of glutathione-capped gold nanoclusters for sensing and imaging of alkaline phosphatase-mediated hydrolysis of adenosine triphosphate, Nanoscale 10 (2018) 17691–17698.
[31] T. Zhao, N. Goswami, J. Li, Q. Yao, Y. Zhang, J. Wang, D. Zhao, J. Xie, Probing the microporous structure of silica shell via aggregation-induced emission in Au(I)-thiolate@SiO2 nanoparticle, Small 12 (2016) 6537–6541.
[32] J.P. Vanegas, E. Zaballos-García, M. González-Béjar, P. Londoño-Larrea, J. Pérez-Prieto, Adenosine monophosphate-capped Gold(I) nanoclusters: synthesis and lanthanide ion-induced enhancement of their luminescence, RSC Adv. 6 (2016) 17678–17682.
[33] S.H. Kim, K.L. Kiick, Heparin-mimetic sulfated peptides with modulated affinities for heparin-binding peptides and growth factors, Peptides 28 (2007) 2125–2136.
[34] C.-Y. Lee, W.-L. Tseng, Molecular beacon-based fluorescent assay for specific detection of oversulfated chondroitin sulfate contaminants in heparin without enzyme treatment, Anal. Chem. 87 (2015) 5031–5035.
[35] Z. Wang, J. Lee, A.R. Cossins, M. Brust, Microarray-based detection of protein binding and functionality by gold nanoparticle probes, Anal. Chem. 77 (2005) 5770–5774.
[36] K. Du, S.H. Ko, G.M. Gallatin, H.P. Yoon, J. Alexander Liddle, A.J. Berglund, Quantum dot-DNA origami binding: a single particle, 3D, real-time tracking study, Chem. Comm. 49 (2013) 907–909.
[37] Z. Qian, L. Chai, C. Tang, Y. Huang, J. Chen, H. Feng, Carbon quantum dots-based recyclable real-time fluorescence assay for alkaline phosphatase with adenosine triphosphate as substrate, Anal. Chem. 87 (2015) 2966–2973.
[38] A. Reichert, J.O. Nagy, W. Spevak, D. Charych, Polydiacetylene liposomes functionalized with sialic acid bind and colorimetrically detect influenza virus, J. Am. Chem. Soc. 117 (1995) 829–830.
[39] H. Päkkilä, S. Blom, K. Kopra, T. Soukka, Aptamer-directed lanthanide chelate self-assembly for rapid thrombin detection, Analyst 138 (2013) 5107–5112.
[40] K. Lacina, M. Konhefr, J. Novotný, D. Potěšil, Z. Zdráhal, P. Skládal, Combining ferrocene, thiophene and a boronic acid: a hybrid ligand for reagentless electrochemical sensing of cis-diols, Tetrahedron Lett. 55 (2014) 3235–3238.
[41] E. Farjami, L. Clima, K.V. Gothelf, E.E. Ferapontova, DNA interactions with a methylene blue redox indicator depend on the DNA length and are sequence specific, Analyst 135 (2010) 1443–1448.
[42] B. Viguier, K. Zór, E. Kasotakis, A. Mitraki, C.H. Clausen, W.E. Svendsen, J. Castillo-León, Development of an electrochemical metal-ion biosensor using self-assembled peptide nanofibrils, ACS Appl. Mater. Interfaces 3 (2011) 1594–1600.
[43] X. Xiao, Z. Kuang, J.M. Slocik, S. Tadepalli, M. Brothers, S. Kim, P.A. Mirau, C. Butkus, B.L. Farmer, S. Singamaneni, C.K. Hall, R.R. Naik, Advancing peptide-based biorecognition elements for biosensors using in-silico evolution, ACS Sens. 3 (2018) 1024–1031.
[44] P. Miao, T. Liu, X. Li, L. Ning, J. Yin, K. Han, Highly sensitive, label-free colorimetric assay of trypsin using silver nanoparticles, Biosens. Bioelectron. 49 (2013) 20–24.
[45] K. Kikuchi, S. Hashimoto, S. Mizukami, T. Nagano, Anion sensor-based ratiometric peptide probe for protein kinase activity, Org. Lett. 11 (2009) 2732–2735.
[46] J.S. Park, A. Baek, I.-S. Park, B.-H. Jun, D.-E. Kim, A graphene oxide-based platform for the assay of RNA synthesis by RNA polymerase using a fluorescent peptide nucleic acid probe, Chem. Comm. 49 (2013) 9203–9205.
[47] S. Sharma, H. Byrne, Richard J. O'Kennedy, Antibodies and antibody-derived analytical biosensors, Essays Biochem. 60 (2016) 9–18.
[48] H. Cheng, Y. Liu, Y. Hu, Y. Ding, S. Lin, W. Cao, Q. Wang, J. Wu, F. Muhammad, X. Zhao, D. Zhao, Z. Li, H. Xing, H. Wei, Monitoring of heparin activity in live rats using metal–organic framework nanosheets as peroxidase mimics, Anal. Chem. 89 (2017) 11552–11559.
[49] X. Le Guével, B. Hötzer, G. Jung, K. Hollemeyer, V. Trouillet, M. Schneider, Formation of fluorescent metal (Au, Ag) nanoclusters capped in bovine serum albumin followed by fluorescence and spectroscopy, J. Phys. Chem. C 115 (2011) 10955–10963.
[50] H. Schmidbaur, A. Schier, Aurophilic interactions as a subject of current research: an up-date, Chem. Soc. Rev. 41 (2012) 370–412.
[51] Y.-A. Lee, R. Eisenberg, Luminescence tribochromism and bright emission in gold(I) thiouracilate complexes, J. Am. Chem. Soc. 125 (2003) 7778–7779.
[52] R. Zhan, Z. Fang, B. Liu, Naked-eye detection and quantification of heparin in serum with a cationic polythiophene, Anal. Chem. 82 (2010) 1326–1333.
[53] Y.-T. Wang, W.-L. Tseng, Surfen-assembled graphene oxide for fluorescence turn-On detection of sulfated glycosaminoglycans in biological matrix, ACS Sens. 2 (2017) 748–756.
[54] J.V. Olsen, S.-E. Ong, M. Mann, Trypsin cleaves exclusively C-terminal to arginine and lysine residues, Mol. Cell. Proteom. 3 (2004) 608–614.
[55] W.A. See, J.L. Smith, Urinary levels of activated trypsin in whole-organ pancreas transplant patients with duodenocystostomies, Transplantation 52 (1991) 630–633.
[56] T.U. Hausamen, R. Helger, W. Rick, W. Gross, Optimal conditions for the determination of serum alkaline phosphatase by a new kinetic method, Clin. Chim. Acta 15 (1967) 241–245.
[57] J.S. Desgrosellier, D.A. Cheresh, Integrins in cancer: biological implications and therapeutic opportunities, Nat. Rev. Canc. 10 (2010) 9.
[58] G.K. Ojakian, D.R. Ratcliffe, R. Schwimmer, Integrin regulation of cell-cell adhesion during epithelial tubule formation, J. Cell Sci. 114 (2001) 941–952.
[59] Y. Hu, J. Li, J. Yang, P. Wei, Y. Luo, L. Ding, W. Sun, G. Zhang, X. Shi, M. Shen, Facile synthesis of RGD peptide-modified iron oxide nanoparticles with ultrahigh relaxivity for targeted MR imaging of tumors, Biomater. Sci. 3 (2015) 721–732.
[60] Y. Xiao, Q. Zhang, Y. Wang, B. Wang, F. Sun, Z. Han, Y. Feng, H. Yang, S. Meng,

Please cite this article as: J.-G. You, W.-L. Tseng, Peptide-induced aggregation of glutathione-capped gold nanoclusters: A new strategy for designing aggregation-induced enhanced emission probes, Analytica Chimica Acta, https://doi.org/10.1016/j.aca.2019.05.069

Z. Wang, Dual-functional protein for one-step production of a soluble and targeted fluorescent dye, Theranostics 8 (2018) 3111–3125.
[61] C. Ding, Y. Xu, Y. Zhao, H. Zhong, X. Luo, Fabrication of BSA@AuNC-based nanostructures for cell fluoresce imaging and target drug delivery, ACS Appl. Mater. Interfaces 10 (2018) 8947–8954.
[62] Q. Liu, J. Wang, B.J. Boyd, Peptide-based biosensors, Talanta 136 (2015) 114–127.
[63] A. Karimzadeh, M. Hasanzadeh, N. Shadjou, M.d.l. Guardia, Peptide based biosensors, Trends Anal. Chem. 107 (2018) 1–20.

Please cite this article as: J.-G. You, W.-L. Tseng, Peptide-induced aggregation of glutathione-capped gold nanoclusters: A new strategy for designing aggregation-induced enhanced emission probes, Analytica Chimica Acta, https://doi.org/10.1016/j.aca.2019.05.069